Photocontrol of Protein Folding: The Interaction of Photosensitive Surfactants with Bovine Serum Albumin†

C. Ted Lee, Jr.,*,‡ Kenneth A. Smith, and T. Alan Hatton*

Department of Chemical Engineering, Massachusetts Institute of Technology, Cambridge, Massachusetts 02144

Received July 8, 2004; Revised Manuscript Received October 19, 2004

ABSTRACT: The photoresponsive interaction of light-sensitive azobenzene surfactants with bovine serum albumin (BSA) at neutral pH has been investigated as a means to control protein folding with light irradiation. The cationic azobenzene surfactant undergoes a reversible photoisomerization upon exposure to the appropriate wavelength of light, with the visible-light (trans) form of the surfactant being more hydrophobic than the UV-light (cis) form. As a consequence, the trans form exhibits enhanced interaction with the protein compared to the cis form of the surfactant, allowing photoreversible control of the protein folding/unfolding phenomena. Small-angle neutron-scattering (SANS) measurements are used to provide detailed information on the protein conformation in solution. A fitting of the protein shape to a low-resolution triaxial ellipsoid model indicates that three discrete forms of the protein exist in solution depending on the surfactant concentration, with lengths of approximately 90, 150, and 250 Å, respectively, consistent with additional dynamic light-scattering measurements. In addition, shape-reconstruction methods are applied to the SANS data to obtain relatively high-resolution conformation information. The results confirm that BSA adopts a heart-shaped structure in solution at low surfactant concentration, similar to the well-known X-ray crystallographic structure. At intermediate surfactant concentrations, protein elongation results as a consequence of the C-terminal portion separating from the rest of the molecule. Further increases in the surfactant concentration eventually lead to a highly elongated protein that nonetheless still exhibits some degree of folding that is consistent with the literature observations of a relatively high helical content in denatured BSA. The results clearly demonstrate that the visible-light form of the surfactant causes a greater degree of protein unfolding than the UV-light form, providing a means to control protein folding with light that, within the resolution of SANS, appears to be completely reversible.

Protein folding is a remarkable process that affects nearly every aspect of biological function. The conformation of a protein in solution is generally a function of electrostatic, hydrogen-bonding, van der Waals, and hydrophobic interactions among the amino acid residues that all typically favor a folded conformation, overcoming the entropic penalty associated with this folding of the protein into a compact state. For a given amino acid sequence, the protein will often adopt a unique structure in solution, termed the native state, whereby the charged and polar amino acid groups are exterior and exposed to water, while the nonpolar moieties generally reside in the interior of the folded structure, protected from unfavorable solvent interactions. Protein unfolding can be induced by a variety of external conditions such as changes in pH (ionization of nonpolar residues), temperature (complex interplay between enthalpic and entropic effects), and pressure (a consequence of a negative volume change upon protein folding), or through the addition of a chemical denaturant (preferential interaction of both the polar and nonpolar amino acids with the denaturant rather than with water) (*1*).

In addition, a variety of studies have demonstrated that proteins can unfold in response to the addition of surfactants (*2*−*4*). Ionic surfactants bind strongly to proteins through electrostatic interactions between the surfactant headgroups and oppositely charged amino acids, and through hydrophobic interactions between the surfactant tails and nonpolar amino acids. As a result, surfactant binding often results in protein unfolding, because of the fact that the hydrophobic amino acids no longer need to reside in the protein core hidden from water. This effect of screening the water−nonpolar amino acid interaction with surfactant has been utilized for decades in the well-known sodium dodecyl sulfate−polyacrylamide gel electrophoresis (SDS−PAGE)[1] technique, whereby the anionic SDS surfactant is used to unfold the protein into a polypeptide chain, thereby allowing separation based predominantly on molecular weight.

Despite the fact that interactions between proteins and surfactants are industrially, scientifically, and biologically

† We would also like to acknowledge the Cambridge−MIT Institute for support of this research.

* To whom correspondence should be addressed. E-mail: tedlee@usc.edu (C.T.L.); tahatton@mit.edu (T.A.H.).

‡ Current address: Department of Chemical Engineering, University of Southern California, Los Angeles, CA 90089.

[1] Abbreviations: BSA, bovine serum albumin; SANS, small-angle neutron scattering; SDS, sodium dodecyl sulfate; azoTAB, azobenzene trimethylammonium bromide surfactant; PDDF, pair distance distribution function; DLS, dynamic light scattering; DTAB, dodecyltrimethylammonium bromide.

10.1021/bi048556c CCC: $30.25
Published on Web 12/21/2004

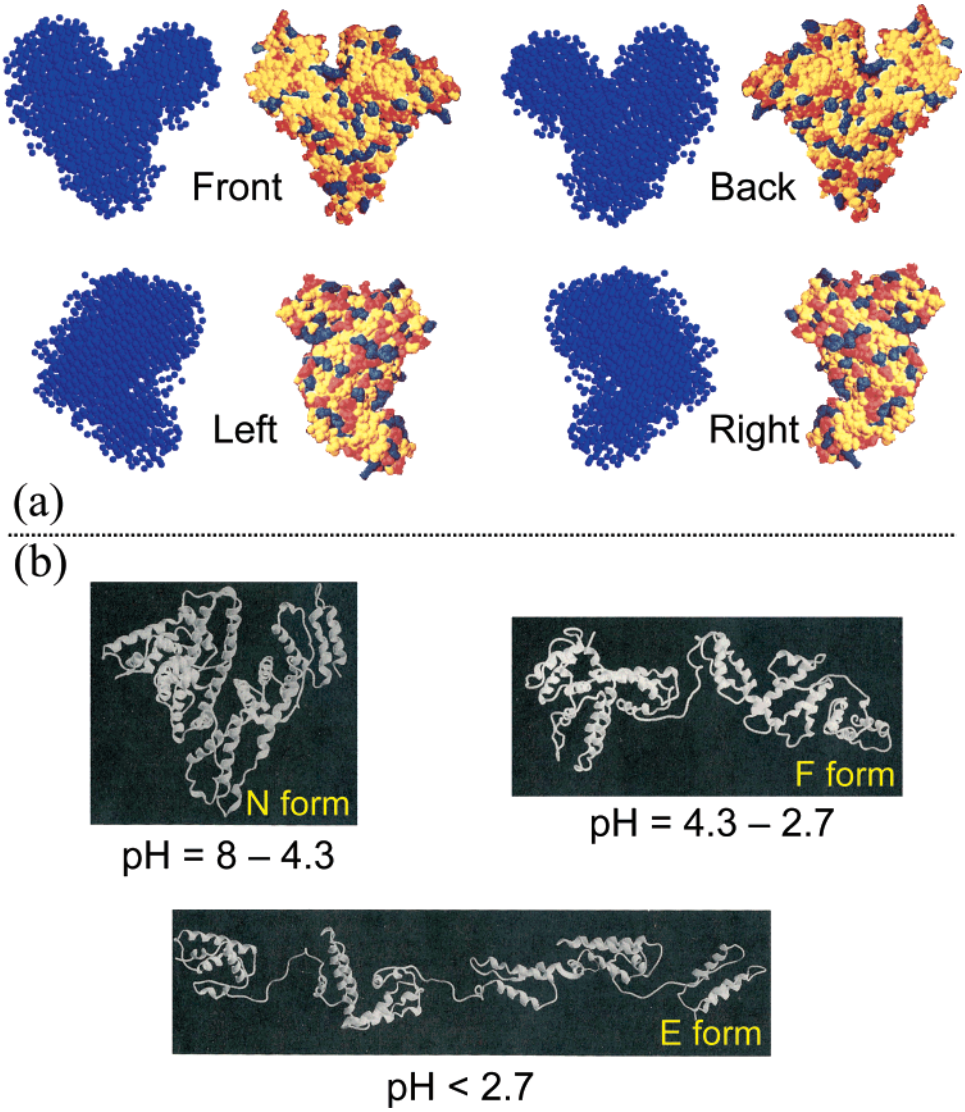

FIGURE 1: Comparison of the structure of BSA determined from SANS (this paper, in blue) with the (a) space-filling model and (b) proposed ribbon diagrams of serum albumin from Carter and Ho (*12*).

important, the structure of the resulting protein−surfactant complexes is still debated. A variety of structures have been proposed for these complexes at high surfactant concentration (*2*, *4*), including the "necklace and bead model" in which surfactant micelles are arranged along a flexible polypeptide chain (*5*), the "rodlike-particle model", where the protein expands into a high aspect ratio prolate ellipsoid upon surfactant binding (*6*, *7*), and the "flexible cylindrical micelle model", where the protein molecule wraps around the surfaces of cylindrical micelles (*8*). The most-likely structure emerging from the literature is one of a fractal arrangement of relatively small surfactant micelles bound to an extended protein polypeptide chain, similar to the necklace model (*4*, *9*−*11*), with the helical portions of the protein contained within the hydrophobic micelle cores (*2*). Protein conformations at low surfactant concentrations, however, are less well-studied, and the mechanism by which the folded native form of the protein expands into a "necklace", as well as the intermediate structures between the compact and expanded states, is still debatable.

Bovine serum albumin (BSA) is perhaps the most widely used and best-characterized protein in studies of interactions with surfactants, perhaps because of the relatively large number (*12*) of charged amino acids on the surface of BSA (net charge of −18 at neutral pH) (*13*). The primary structure of BSA consists of nine loops held together by 17 disulfide bonds, resulting in three domains (I, II, and III) each containing two subdomains or alternatively each containing one small and two large loops (*12*, *14*, *15*). These loops are composed largely of helical segments, resulting in about two-thirds of the molecule exhibiting helical content. Early works describe the conformation of BSA in solution at neutral pH as a prolate ellipsoid, based on a variety of experimental techniques [e.g., hydrodynamic (*16*−*20*), small-angle scattering (*21*, *22*), and electron microscopy(*23*)]. Unfortunately, this "incorrect" (*12*) view has persisted and is still commonly used in the literature, even with the majority of contemporary evidence (*11*, *24*), corroborated in this work, pointing to a "heart-shaped" structure in solution (triangular shape with 80 Å edges and 30 Å thick), similar to that obtained from X-ray crystallography (*25*) (see Figure 1). Two additional conformations of BSA are observed with decreasing pH, beginning with the heart-shaped normal "*N*" form at neutral pH, followed by the fast "*F*" form (40 × 129 Å) below a pH of about 4, and concluding with the expanded "*E*" form (21 × 250 Å) for pH less than about 3 (*12*, *15*). The $N \rightarrow F$

transition is typically associated primarily with an unfolding of domain III or the C-terminus portion (upper left-hand side of the "front" view in Figure 1) (*15*) from the rest of the molecule, with domains I and II remaining relatively intact (*12*, *26*−*28*). During the $F \rightarrow E$ transition, all six subdomains are generally thought to separate from the compact structure; however, a relatively high helical content (∼ 50%) is still observed (*28*), suggesting that the loops remain intact. On the basis of studies using BSA fragments, it has also been suggested that cooperative surfactant binding occurs primarily between the loop segments, while "SDS denaturation does not disrupt the helices formed in the six large loops" (*29*).

In the present work, we show that light can be used as a novel method of controlling protein structure. This is achieved through the use of a light-responsive azobenzene surfactant, which undergoes a reversible trans ↔ cis photoisomerization upon exposure to visible or UV light (*30*−*34*). The trans (planar) form of the surfactant is more hydrophobic than the cis (bent) form as a result of the larger dipole moment across the azo group in the nonplanar form (*34*). As a consequence, hydrophobic interactions between the surfactant and protein can be tuned with light illumination. Light-scattering and neutron-scattering data are used to show that the trans from of the surfactant causes a greater degree of protein unfolding than the cis form and that these changes in protein structure are photoreversible. Shape reconstruction is applied to the small-angle neutron-scattering (SANS) data, allowing for relatively high-resolution "images" of the protein structure to be obtained throughout the unfolding process as a function of the surfactant concentration and light illumination. These results are compared to low-resolution triaxial ellipsoid fits of the SANS data and to results extracted from dynamic light-scattering (DLS) data, to provide a consistent view of the nature of surfactant-induced protein elongation, as well as the mechanism of photoreversible control of protein folding.

MATERIALS AND METHODS

Materials. An azobenzene trimethylammonium bromide surfactant (azoTAB) of the form shown below was synthesized according to published procedures (*30*, *34*), with a purity of 99% as determined by gas chromatography and NMR. Photoisomerization of azoTAB was done as previously described (*35*). Briefly, conversion from the trans to the cis form of azoTAB was achieved by illuminating stirred solutions with the 365 nm UV line from a 200 W Mercury arc lamp (Oriel, model no. 66942) isolated using a 320 nm band-pass filter (Oriel, model no. 59800). For conversion from the cis to the trans form, a 400 nm long-pass filter (Oriel, model no. 59472) was used to isolate the 436 nm line of the mercury lamp. A heat-absorbing filter (Oriel, model no. 59042) was placed in the beam path to absorb the IR light produced by the lamp. It should be noted that absorption measurements indicate that under visible-light conditions the surfactant exhibits an approximately 75:25 trans/cis equilibrium, while under UV light, the surfactant is primarily of the cis form (we were unable to deconvolute the presumably small trans peak). Throughout this paper, the terms "trans form" and "cis form" indicate that the surfactant is primarily trans or cis, respectively.

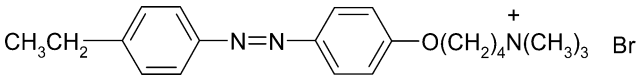

Highest-quality lyophilizate BSA, guaranteed monomeric for 1 year as a solid and for 6 months in solution, was purchased from Roche and used as received. The low ionic strength phosphate buffer (pH 7.2, 8.3 mM) was obtained from Sigma. All other chemicals were obtained from Aldrich. A protein concentration of 10 mg/mL was employed in the neutron-scattering experiments, while a concentration of 0.66 mg/mL was used for the light scattering and fluorescence measurements (see below).

Light-Scattering Measurements. DLS measurements at 25 °C were performed at an angle of 90° on a Brookhaven model BI-200SM instrument (Brookhaven Instrument Co.) with an argon ion laser operating at 514 nm. A relatively low laser power (<100 mW) was used to avoid conversion of the azoTAB cis isomer into the trans form during the course of the experiments. The data were analyzed with both the NNLS and CONTIN routines (difference < 2 Å) using a BI-9000AT digital correlator (Brookhaven Instrument Corp.). The protein-buffer solutions were passed through a 0.2 μm filter prior to the measurements, while the surfactant was added after filtration to avoid loss of the surfactant through adsorption on the membrane. A lower protein concentration (10^{-5} M or 0.66 mg/mL) was used in the light-scattering experiments to measure the infinite dilution diffusion coefficient of the protein more accurately.

SANS. The SANS data were collected on the 30-m NG-3 instrument at NIST (*36*) using a neutron wavelength of $\lambda =$ 6 Å at 25 °C. Two sample−detector distances were employed (1.33 and 7.0 m), combined with a 25 cm offset of the detector, to give a Q range of $Q = 4\pi\lambda^{-1}\sin(\theta/2) = 0.0048$ Å^{-1} − 0.46 Å^{-1}, where θ is the scattering angle. The net intensities were corrected for the background and "empty" cell (pure D_2O), followed by accounting for the detector efficiency using the scattering from an isotropic scatterer (plexiglass), and then converted to an absolute differential cross section per unit sample volume (in units of cm^{-1}) using an attenuated empty beam. The coherent intensities of the sample were obtained by subtracting the incoherent contribution from the hydrogen atoms in BSA (0.0034 cm^{-1}) and the surfactant (0−0.0012 cm^{-1}).

The SANS data were analyzed using three complementary techniques: calculation of the pair distance distribution functions (PDDFs), modeling the protein shape as a triaxial ellipsoid, and use of a relatively new shape-reconstruction algorithm. The PDDFs were calculated assuming a monodisperse system using GNOM (*37*) over a Q range of ca. 0.025 Å^{-1} − 0.3 Å^{-1}; data at lower Q values were not used in these calculations to avoid the need to account for the effects of particle interactions in the analysis. The lowest maximum particle diameter (D_{max}) was selected to be that which gave a smooth return of the PDDF to 0 at D_{max}. For the triaxial ellipsoid model, the SANS intensity $I(Q)$ was fit to a model of the form

$$I(Q) = \phi(\Delta\rho)^2 V_P \langle F^2(Q)\rangle_0 S(Q) + I_b$$

where ϕ is the volume fraction of the protein−surfactant complex, $V_P = (4/3)\pi abc$ is the volume of the triaxial ellipse

with half-axes a, b, and c equal to half of the thickness, width, and length, respectively, and I_b is the background scattering intensity. The neutron scattering length density difference $\Delta\rho$ between the protein and the D_2O solvent was set to a value of 2.47×10^{-6} Å^{-2}, based on the reported value of the scattering length density of BSA of 3.89×10^{-6} Å^{-2} in D_2O (*38*). The form factor was calculated (*39*−*41*) by averaging over all possible protein orientations by integrating over the angles φ and θ

$$\langle F^2(Q)\rangle_0 = \frac{2}{\pi}\int_0^{\pi/2}\int_0^{\pi/2} F^2[Q,r(a,b,c,\varphi,\theta)] \sin\varphi \, d\varphi \, d\theta$$

with

$$F(Q,r) = 3[\sin(Qr) - Qr\cos(Qr)]/(Qr)^3$$

and

$$r(a,b,c,\varphi,\theta) = [(a^2\sin^2\theta + b^2\cos^2\theta)\sin^2\varphi + c^2\cos^2\varphi]^{1/2}$$

For the structure factor $S(Q)$, either a mean spherical approximation accounting for electrostatic repulsions (*42*, *43*) or a square-well potential representing short-ranged attractions (*44*) was used, depending on the degree of protein neutralization by the surfactant (see below). The depth ($\epsilon' = 3.28k_BT$) and width ($\lambda = 1.033$) of the square well were estimated from the van der Waals attractive potential (*45*) by equating the area in the "well" to that of the overall potential (van der Waals plus electrostatic) over the range of separation distances where the potential is attractive. The model fits were performed using the data analysis software and structure factors provided by NIST (triaxial form factor available from CTL upon request). The data were fit up to a maximum Q value of 0.4 Å^{-1}, beyond which the data exhibited unsatisfactory noise. The shape reconstructions were performed using GA_STRUCT generously supplied by Dr. William Heller (*46*). A Q range of 0.02−0.3 Å^{-1} was employed, with 2000 points used to describe the protein shape. The lower cutoff value of 0.02 Å^{-1} was used to ensure that only the particle shape (form factor) and not the particle−particle interactions (structure factor) were used in the shape reconstruction analysis. For the N and F forms of BSA, the protein conformations reported below are the "consensus envelopes" that GA_STRUCT automatically produces from the average of 10 different runs. For the highly unfolded E form, however, the individual conformations from each run, while being similar in the degrees of elongation and "kinking" (see below), contained enough variation so as to yield average structures that were somewhat blurred, washing out many of the salient features of the folding observed in the individual runs. Thus, only the structure for the run best fitting the data is typically shown to save space.

Fluorescence Measurements. Fluorescence measurements using Nile Red as the probe were performed on a TimeMaster Fluorescence Lifetime spectrometer (Photon Technology International) in steady-state mode at 25 °C. The results were obtained with an excitation wavelength of 575 nm using an excess amount of the solid dye, with saturation assured by sonicating the mixtures for 15 min followed by stirring for several days. Samples were then centrifuged prior to loading into the cuvette to prevent the inclusion of solid Nile Red.

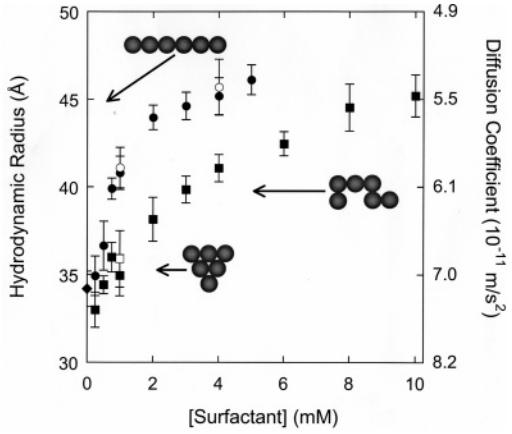

FIGURE 2: BSA unfolding versus azoTAB surfactant concentration as measured by DLS at 25 °C under both visible (●) and UV (■) light illumination, as well as the data for pure BSA (◆). Open symbols are used to demonstrate the photoreversible changes in protein conformation upon visible → UV → visible (○) and UV → visible → UV (□) exposure.

The fluorescence spectra were collected in front-face mode by placing the cuvette at an angle of ca. 50° from the incident light, thereby allowing the emission spectra to be obtained at relatively large optical densities (OD > 1) without complications arising from absorption. To minimize the effect of reflected light, a horizontally polarized filter was placed just before the photomultiplier tube. The slit widths for excitation and emission were 1 and 2 nm, respectively.

RESULTS AND DISCUSSION

BSA Conformation Changes with Light (DLS). The effect of azoTAB surfactant binding and light illumination on the conformation and folding of BSA is shown in the DLS results in Figure 2. Increasing the amount of the trans or cis forms of the surfactant causes the measured diffusion coefficient of the surfactant−BSA complex to decrease, an indication of an increase in the overall size of the complex. This is evidenced by examining the effective hydrodynamic radius calculated from the Stokes−Einstein equation, namely, $R_H = k_BT/6\pi\eta D$, where k_B is Boltzmann's constant, T is the temperature, η is the viscosity of the solvent, D is the infinite dilution diffusion coefficient obtained at low concentration, and R_H is the hydrodynamic radius assuming a spherical shape.

The value of the hydrodynamic radius of BSA obtained without the surfactant (34 Å) is in excellent agreement with values from the literature (*9*, *47*−*52*) (typically ∼34 ± 3 Å) at similar conditions. Upon increasing the concentrations of both the trans and cis forms of the surfactant, the size of the BSA−surfactant complex increases as a result of protein unfolding. The trans form of the surfactant results in a more rapid increase in the size of the complex than does the cis form, indicating that the more hydrophobic trans-azoTAB has a greater tendency than the relatively hydrophilic cis form to bind to the protein. This allows for reversible, light-directed changes in the size of the BSA−surfactant complex, as shown in Figure 2, because the hydrophobic interactions between surfactant tails and the nonpolar amino acids (that are normally folded into the interior of the protein) can be tuned with light illumination. A similar unfolding of BSA has been observed with increases in SDS or dodecyltrim-

ethylammonium bromide (DTAB) concentrations with DLS (*49*, *52*), with the maximum hydrodynamic radius measured in Figure 2 consistent with observed values from these studies. Furthermore, as the hydrophobicity of traditional surfactants is increased through the use of longer hydrocarbon tails, BSA structural changes have been observed to occur at lower surfactant concentrations (*29*), analogous to a greater degree of unfolding for the more hydrophobic trans form of azoTAB. In contrast to these traditional surfactant effects, however, the photoinduced changes in the size of BSA upon UV- or visible-light illumination were observed to be completely reversible within the experimental uncertainty, as seen in Figure 2.

For illustrative purposes and for reasons that will become clear below during analysis of the SANS data, diffusion coefficients (i.e., effective hydrodynamic radii) for different potential conformations of BSA were estimated as shown in Figure 2. These values were calculated from the theory of Kirkwood (*53*, *54*) by treating the protein as a chain of six equivalent spherical subunits, a reasonable assumption for BSA that is known to have three domains each containing two subdomains (*12*, *14*, *15*). Each subunit was assumed to be a compact sphere using the minimum radius possible for the subunit molecular weight (i.e., $R_{min} = 0.66\ MW^{1/3} = 15$ Å) with the addition of a 3 Å thick water hydration shell. As seen in the graph, the increase in the hydrodynamic radius is consistent with protein unfolding and separation of the six protein subdomains. The initial triangle-like structure shown in Figure 2, with a thickness of 30 Å and a side length of about 90 Å, roughly corresponds to the shape and dimensions of the heart-shaped structure of BSA determined from X-ray crystallography (*25*) (30 Å thick and 80 Å on edge), while the fully extended structure hypothesized at higher surfactant concentrations is compatible with the low-pH threadlike form (21 × 250 Å) observed with electron microscopy (*55*).

It is important to note that the increase in hydrodynamic radius (or the decrease in the measured diffusion coefficient) observed in Figure 2 cannot simply be a result of the increase in the effective mass of the surfactant−protein complex that occurs with surfactant binding. For example, preliminary binding isotherms (not shown) indicate that at this low BSA concentration, only about seven surfactant molecules are bound per protein at 1 mM azoTAB surfactant under visible light, consistent with the reported values of 4−11 high-affinity binding sites observed in other cationic surfactant−BSA systems (*56*, *57*). This gives an increase in the mass of the surfactant−protein complex that occurs with surfactant binding of approximately 6%. For globular proteins with a compact spherical shape, the radius is expected in increase with $MW^{1/3}$, accounting for only a 2% increase in the measured hydrodynamic radius with surfactant binding (compared to an increase from 34 Å for pure BSA to 40 Å at 1 mM azoTAB under visible light). Thus, it is clear that conformational changes and not simply an increase in the effective mass are responsible for the observed increase in size of the BSA−surfactant complex.

BSA Conformation Changes with Light (SANS). Although the above DLS measurements illustrate that reversible changes in the expanded (unfolded) nature of the protein can be induced with light illumination, the measured diffusion coefficients cannot distinguish between the many different

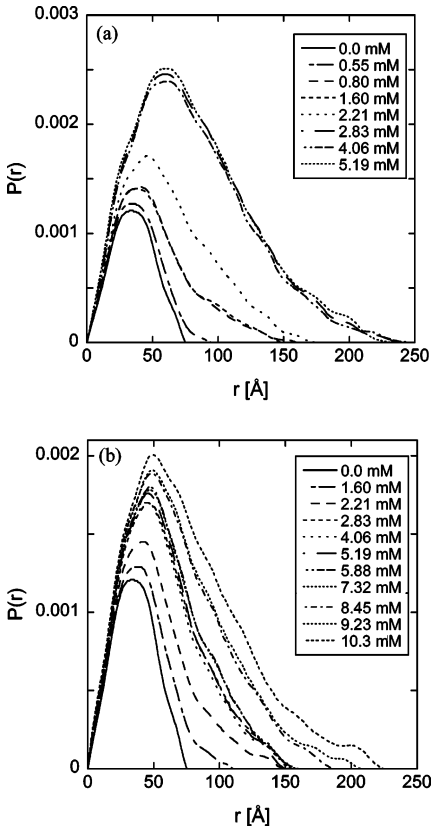

FIGURE 3: PDDFs of BSA−azoTAB solutions as a function of the surfactant concentration under both (a) visible- and (b) UV-light illumination.

expanded states of the protein that could possibly occur upon surfactant binding. In contrast, the relatively wide Q range utilized in a typical SANS experiment (in this case $Q = 0.005$ Å^{-1} − 0.45 Å^{-1}) allows a wide range of length scales $L \propto 2\pi/Q$ to be investigated simultaneously. For example, changes in the thickness of the BSA molecule (∼30 Å) would be observed around $Q = 0.21$ Å^{-1}, while an increase in the length of BSA to previously reported TEM values of up to 250 Å would be seen at ca. $Q = 0.025$ Å^{-1}, a difference of about a decade in the Q range. This simple example points to the utility of SANS in studying protein structure in solution.

In the sections that follow, the SANS data collected from BSA−azoTAB systems will be analyzed in three distinct ways. The first technique employed will be the calculation of PDDFs, a model-independent method used to qualitatively investigate protein unfolding. This will be followed with fitting of the SANS data by assuming the protein adopts a triaxial ellipsoidal shape in solution and interacts through either electrostatic repulsive or square-well attractive interactions. In the final technique, shape-reconstruction analysis will be used to investigate protein shape with a greater resolution than the triaxial fits. Each of these methods gives consistent results, allowing precise determination of the mechanisms of light-directed protein folding and unfolding.

PDDFs. To investigate the effect of surfactant and light illumination on protein structure, the PDDFs shown in Figure 3 were calculated from the experimental scattering data (see below). Because the PDDF is a measure of the probability $P(r)$ of finding two scattering centers at a distance r apart (*40*, *58*), information about protein conformation can be

readily obtained using a model-independent, straightforward procedure. Thus, calculation of the PDDF is a commonly employed technique to probe the myriad of complex structures that proteins can adopt in solution. For example, the PDDF of a globular (i.e., spherical) protein is expected to have a symmetric, inverse parabolic shape, with the peak position and the maximum dimension (D_{max}, i.e, the r value beyond which $P(r)$ equals 0) corresponding approximately to the protein radius and diameter, respectively. However, as the protein unfolds, the PDDF will exhibit a tail at larger r, with D_{max} corresponding to the length of the elongated protein.

From Figure 3, it appears that, in the absence of the surfactant, BSA adopts a predominantly globular structure, with the PDDF exhibiting a maximum at 34 Å, while D_{max} = 75 Å, similar to the pure BSA values determined using SAXS (*11*). These values also closely match the hydrodynamic radius of 34 Å measured in Figure 2, as well as the oft-reported 80 Å edge of the equilibrium triangle approximating the X-ray crystallographic structure (see Figure 1). Upon increasing the concentrations of both the trans and cis forms of the surfactant, a significant extension of the PDDF to larger maximum dimensions occurs, an indication of elongation of the protein upon unfolding. Furthermore, it appears that this unfolding may be a stepwise rather than a gradual transition. This is particularly evident under visible-light illumination, where three discrete protein conformations are observed upon increasing the trans surfactant concentration, with significant unfolding occurring between 0.55 and 0.80 mM and then again in the range of 1.60−2.83 mM. This mechanism is consistent with the *N*, *F*, and *E* forms of BSA observed with decreases in pH. Under UV-light illumination, the stepwise nature of the protein unfolding/elongation process with cis surfactant concentration is less clear, although it appears that again three discrete forms of the protein exist, with maximum dimensions in this case of approximately <100, 150, and 200 Å, respectively. It is important to note that SANS measures the rotational and conformational average of the protein structure, making it difficult to distinguish between intermediately folded states and conditions where a mixture of two equilibrium forms exist simultaneously in solution.

At a minimum, the PDDFs reveal significant unfolding and elongation of BSA with the addition of azoTAB, as well as the ability to control the degree of unfolding with UV−visible-light illumination. In the sections that follow, we will employ two different techniques to analyze the SANS data to further study the protein unfolding in a more quantitative manner. In the first technique, the data will be fit to a low-resolution model consisting of a triaxial ellipsoid form factor with protein interactions being handled through the use of either a rescaled mean spherical approximation of Coulombic repulsive interactions (*42*, *43*) or a square-well attraction potential (*44*). In the second technique, we will employ a model-independent algorithm developed by Heller (*46*) that allows the approximate conformation of the protein to be reconstructed from the SANS data without an *a priori* assumption of the protein shape, within a resolution as small as 5 Å (*59*).

Triaxial Ellipsoid Model. The SANS experimental data, along with fits using a triaxial ellipsoid model of the protein shape, are displayed in Figure 4, with the results of the model

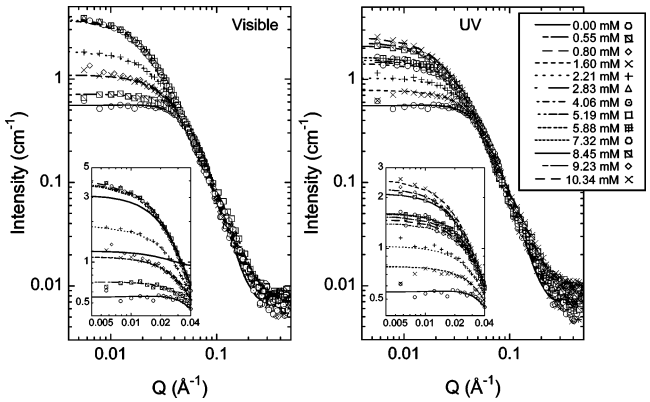

FIGURE 4: SANS data and triaxial fits for BSA−azoTAB solutions as a function of the surfactant concentration. The insets magnify the low-Q region to highlight the effect of protein elongation. Also shown in the inset for visible-light illumination are the normalized form factor, $\phi(\Delta\rho)^2V_P\langle F^2(Q)\rangle_0$, and structure factor, $S(Q)$, at 5.19 mM azoTAB.

fits given in Table 1. Noteworthy is the model fit of the surfactant-free data for pure BSA in pH 7.2 buffer, which consistently attributed an oblate ellipsoid (disklike) structure to BSA. This was true despite our best efforts to "force" a prolate ellipsoid fit with initial guesses and seems to support the assertion by Carter et al (*12*). that BSA is not cigar-shaped at neutral pH in surfactant-free solutions as is often claimed. Note that the SANS data in the present work extend to higher Q values (or equivalently smaller length scales) than other published small-angle scattering data of BSA (Q_{max} < 0.2 Å^{-1}) typically used to conclude that BSA is a prolate ellipsoid (*21*, *22*, *38*, *60*, *61*). This extended Q range may account for the present ability to detect the thin, relatively flat structure expected if BSA adopts a conformation in solution similar to that obtained from X-ray crystallography data (30 Å thick, see Figure 1).

With increases in the trans or cis surfactant concentrations, the scattering intensity increases primarily for Q < 0.05 Å^{-1}, while only modest differences are found at larger Q values. While an increase in low Q scattering is often a characteristic of protein aggregation, this does not appear to be the case here because the formation of aggregates should also lead to a decrease in the scattering at higher Q as the number of independent monomers is diminished (*62*). Therefore, the increase in scattering below Q = 0.05 Å^{-1} ($L \sim 2\pi/Q$ = 125 Å) is most likely consistent with BSA elongation, as shown in the model fits in Table 1 that indicate that the dominant change in the BSA conformation is in the triaxial ellipsoid length (∼100 Å − 250 Å or Q < 0.025 Å^{-1} − 0.063 Å^{-1}), while the thickness (∼25 Å or Q = 0.25 Å^{-1}) and width (∼100 Å or Q = 0.063 Å^{-1}) are relatively unchanged. This observation is also consistent with the six protein subdomains remaining intact but separating from each other as the protein elongates, as has been commonly observed during the $N \rightarrow F \rightarrow E$ transitions. Again, it appears that three discrete protein conformations are observed with trans (corresponding to the concentration ranges of <0.55, 0.80−2.21, and >2.83 mM) or cis (with concentration ranges of <1.60, 2.21−7.32, and >8.45 mM) surfactant. It is also important to note that the dimensions of these three forms shown in Table 1, i.e., approximately (30 × 90 × 90 Å), (30 × 90 × 150 Å), and (25 × 100 × 200−250 Å), are consistent with literature values of the N (30 × 80 × 80 Å),

Table 1: Fits of the SANS Data of 1.0 wt % BSA Solutions as a Function of the azoTAB Concentration at 25 °C Using a Triaxial Ellipsoid Form Factor and a Structure Factor Accounting for Either Electrostatic Repulsions or Hard-Sphere Attractions

[surf] (mM)	ϕ	thick (Å)	width (Å)	length (Å)	form	R_g (Å)	D_{max} (Å)	$\lvert z^{eff}\rvert$	Bkg. (cm^{-1})	$\chi^2/(N-1)$
0	0.0094	28.4	92.7	92.3	*N*[a]	27.5[b]	75[b]	7.60	0.0034	2.65
				Visible Light						
0.55	0.0100	27.4	95.9	96.0	*N*	29.5	95	3.84	0.0047	2.08
0.80	0.0103	27.0	84.4	161	*F*	42.0	160	0.001	0.0042	2.54
1.60	0.0103	26.8	83.3	161	*F*	42.2	150	0.001	0.0044	2.36
2.21	0.0103	27.5	91.9	190	*F*	49.9	180		0.0048	2.61
2.83	0.0126	23.9	128	268	*E*	66.0	245		0.0034	5.68
4.06	0.0116	25.2	128	263	*E*	65.8	250		0.0034	4.37
5.19	0.0137	22.6	123	253	*E*	66.0	240		0.0041	5.78
				UV Light						
1.60	0.0093	28.7	87.8	116	*N*	32.5	110	3.68	0.0036	2.73
2.21	0.0093	29.1	89.4	147	*F*	40.7	150	1.10	0.0038	3.11
2.83	0.0097	28.9	103	142	*F*	45.8	160		0.0041	4.93
4.06	0.0095	29.4	102	138	*F*	45.6	160		0.0045	4.31
5.19	0.0098	28.8	103	144	*F*	45.1	160		0.0049	4.22
5.88	0.0103	27.4	105	149	*F*	46.4	155		0.0052	4.01
7.32	0.0103	27.6	103	155	*F*	46.5	160		0.0051	3.93
8.45	0.0115	25.0	101	190	*E*	53.6	190		0.0062	3.84
9.23	0.0112	25.3	103	208	*E*	55.9	210		0.0058	3.90
10.34	0.0122	23.6	105	224	*E*	62.0	225		0.0065	3.42

[a] Proposed form of BSA in solution (see also Figure 6). [b] Determined using GNOM (see the text).

F (40 × 129 Å), and *E* (21 × 250 Å) forms of BSA observed with decreases in pH through X-ray crystallography (*25*) and electron microscopy (*55*). The modest differences between the fitted dimensions and those from literature and particularly the relatively large values of semiaxis *b* in the (*a* × *b* × *c*) triaxial ellipsoids for the *F* and *E* forms can likely be attributed to the fact that an ellipsoid is widest at the center and tapers at the ends. Thus, the fitted and experimental dimensions are in reasonable agreement, suggesting that BSA adopts a form in solution similar to that observed with these solid-state measurements. Similar correlations between the crystal and solution structure have been noted in the literature for various proteins (*46, 59, 63*−*68*).

Of importance is the fact that at a constant surfactant concentration, the conformation of BSA can be controlled with light. For example, at 5.19 mM of azoTAB, BSA adopts a structure similar to the *E* form under visible-light illumination, while irradiating this solution with UV light causes BSA to refold into the *F* form. This photoreversible unfolding and refolding is consistent with literature studies of the unfolding of BSA upon the addition of a variety of sodium *n*-alkyl sulfate and *n*-alkyl trimethylammonium bromide surfactants (*29*). In general, protein unfolding was observed to occur at increasingly lower surfactant concentrations as the length of the alkyl tail increased, indicating that hydrophobic surfactant−protein interactions play an important role in the binding/unfolding process. Thus, the more hydrophobic trans form of azoTAB is expected to result in a greater degree of BSA unfolding than the less hydrophobic cis form. Figure 5 demonstrates that the photoinduced refolding of BSA on going from the trans to cis surfactant forms upon exposure to UV light can be completely reversed upon reexposure to visible light. As seen in the figure, the scattering data are, within SANS experimental error, identical both before and after the visible → UV → visible illumination, indicating that the protein structure can indeed be photocontrolled reversibly.

As seen in Table 1, treating pure BSA in solution as a triaxial ellipsoid interacting through an electrostatic potential

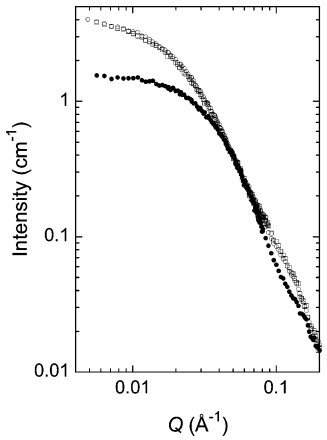

FIGURE 5: Photoreversible control of BSA folding with light. SANS data were taken in the following order: visible light (○) → UV light (●) → visible light (□). [azoTAB] = 4.06 mM.

returns a model fit effective charge of $|z^{eff}| = 7.60$ (note that the model cannot distinguish between a positive or negative charge). This value is in reasonable agreement with the actual net charge of −18 for BSA at neutral pH (*13, 69*), especially when the inherent assumptions involved in treating the protein as a homogeneous ellipsoid with a uniform surface charge distribution (see Figure 1) are considered. As the surfactant concentration is increased, the effective charge decreases rapidly, as expected upon the binding of cationic azoTAB onto the net-negative BSA. Further increases in the trans or cis surfactant concentrations return fitted effective charges of essentially zero, with admittedly slightly lower surfactant−protein ratios (S/P ∼ 5−15) required to "neutralize" BSA than expected based on the −18 net charge. This apparent inconsistency between the SANS model fits and the charge on BSA can be understood by recalling that, in addition to electrostatic repulsions, proteins in solution can also exhibit attractive interactions, a result of a nonuniform charge distribution and various nonpolar and/or noncharged amino acids that can interact through van der Waals, hydrophobic, and hydrogen-

bonding type attractive forces. Neutron-scattering data at low Q are expected to be influenced by both short- and long-ranged correlations between particle positions, and thus, for proteins, the actual structure factor may be a superposition of both attractive and repulsive interactions, which tend to raise or lower the scattering intensity at low Q, respectively.

A precise model for the structure factor of a protein solution that accounts for both attractive and repulsive interactions would be unnecessarily complex, especially given the low-resolution ellipsoid model of the protein shape as well as the nonuniform charge distribution. Thus, we chose to simplify matters by changing from an electrostatic-repulsion to a square-well-attraction structure factor beyond the transition region (i.e., when $z^{\text{eff}} \sim 0$). Although this may introduce some uncertainties in the model fits in the vicinity of the transition region when both attractive and repulsive forces are equally important, it certainly becomes a more accurate assumption at higher surfactant concentrations away from the transition region. It is important to note that the introduction of a square-well attractive interaction has the tendency to *reduce* the fitted length of an ellipsoid, because an increase in either the strength of attraction or the ellipsoid length both increase the low-Q scattering, as seen in the inset of Figure 4 (note that as Q increases beyond 0.04 Å^{-1}, the structure factor oscillates around $S(Q) \sim 1$ to within a few percent). Thus, the elongation of BSA observed in Table 1 is not an artifact of the fitting procedure. The fitted length, however, is somewhat sensitive to the choice of the well depth, with a sensitivity of $\Delta L/\Delta\epsilon' = -1.33$ (%/%), although given that the structure factor correction is small [maximum $S(Q) \sim 1.2$], this sensitivity is relatively mild. The continuity of the particle volume fraction across the transition region, as well as the similarity between this fitted value and the value expected for pure BSA at the concentration used in the experiments, calculated from the literature value of the partial specific volume of BSA (*15*, *70*) along with 0.3 g of bound water per gram of BSA (*71*) ($\phi_{\text{BSA}} = 0.0073 + 0.003 = 0.0103$), serves as a check of the physical significance of the data fits. Furthermore, the increase in ϕ with the surfactant concentration is also consistent with the binding of the surfactant to the protein complex.

The SANS data suggest that no surfactant micelles are formed at the surfactant concentrations used in Figure 4, because there is no interaction peak, which would be characteristic of charged micelles. Beyond a surfactant concentration of ca. 8 mM (trans) or 16−20 mM (cis), however, a peak became evident at $Q_{\text{max}} \sim 0.1$ Å when normalizing the scattering intensities by dividing by the scattering at 5.19 and 10.34 mM, respectively, and the intensity at low Q was observed to decrease (data not shown). Both of these observations suggest the presence of charged species, which could be a result of surfactant micelle formation or an increasingly positive protein net charge because of cationic surfactant binding. The differences between the threshold concentrations for peak formation and the minimum amount of surfactant necessary to achieve the expanded E form of BSA (i.e., 2.83 and 8.45 mM, respectively, which are presumably the amounts of surfactant strongly bound to the protein) indicate that the peak develops when the "excess" surfactant concentration is about 5 mM trans or 10 mM cis, coinciding with the critical micelle concentration values of the two surfactant forms (*30*, *35*).

Thus, we investigated the possibility of micelle formation, either free or bound to the protein, by using a D_2O/H_2O ratio of 40:60, the contrast matching point of BSA (*38*). Despite the fact that the neutron-scattering length density difference between azoTAB and this solvent mixture is relatively high (particularly from the alkyl spacer groups), no excess scattering over the solvent was detected under visible light for either pure BSA or BSA−azoTAB mixtures up to 20 mM surfactant, indicating that micelles are not formed. Attempts to further increase the surfactant concentration resulted in phase separation at 40 mM azoTAB. Therefore, a recharging of the protein at high surfactant concentrations owing to additional surfactant adsorption seems to be the most likely reason for the peak appearance and not micelle formation. Furthermore, an additional structural change may occur in the BSA−surfactant complex beyond an azoTAB concentration of 8 mM. A precise determination of this structure would be complicated by the fact that the protein becomes recharged at elevated surfactant concentrations; preliminary ζ potential measurements (not shown) have confirmed that the net charge of BSA is nearly zero over azoTAB concentrations ranging from 2 to 5 mM under visible light but increases substantially to large positive values as the surfactant concentration is increased beyond this range. Thus, electrostatic interactions will have to be accounted for in any effort to determine the protein conformation at elevated surfactant concentrations. At low surfactant concentrations, where the protein is primarily globular, electrostatic interactions can be accurately modeled using well-known expressions for charged spheres (*42*, *43*), as was done in Table 1. However, as the protein becomes elongated, the assumption of a spherical shape can no longer be applied safely. The challenging task of developing an accurate description of the scattering from charged, highly elongated proteins will be considered in a future study.

Shape Reconstruction. While the model fits above provide convincing evidence of protein conformational changes with increasing surfactant concentration and light illumination, the assumption of a triaxial ellipsoid protein shape provides only low-resolution information on the protein dimensions. More detailed structural information can be obtained using the relatively new technique of "shape reconstruction", whereby the scattering data are fit by treating the protein as a collection of many (a few hundred to a few thousand) spherical scattering centers whose relative positions are altered until agreement is obtained between the simulated scattering and the experimental scattering curves. This approach has been shown to return relatively high resolution (up to 5 Å or $2\pi/Q_{\text{max}}$) (*59*) structural information for proteins. The two most common algorithms for this procedure are GA_STRUCT (*46*) and GASBOR (*59*), both of which are available from the respective authors. In the present work, we have utilized GA_STRUCT, primarily because it features a built-in averaging over 10 separate runs. As an illustration of the quality and precision of structural information that can be obtained from this program, the results of applying GA_STRUCT to the scattering data from a pure BSA solution are compared to the X-ray crystallographic and space-filling model of the protein structure in Figure 1. It is immediately clear that a high degree of similarity exists between the protein structure in solution [fitted using GA_STRUCT, although GASBOR has been shown to yield

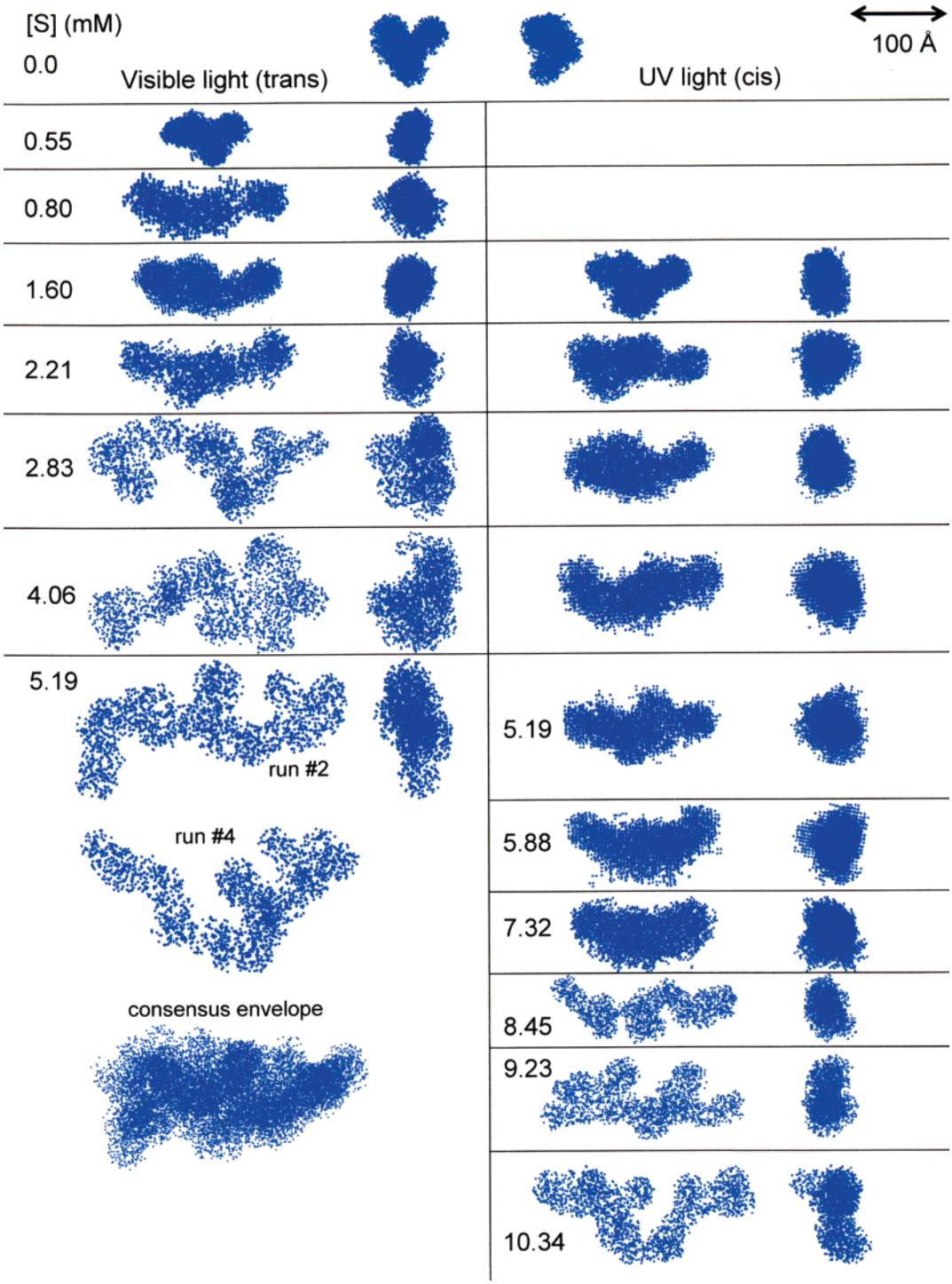

FIGURE 6: Results of shape reconstruction using GA_STRUCT (*46*) as a function of the surfactant concentration and light illumination. Shown are the front and right-side views at each surfactant concentration.

comparable results (*59*)] to that in the solid, crystalline state, in agreement with several reports of the similarity between the crystal and solution structures of a number of proteins. For BSA, this analogy has been somewhat confused because of the persistent but apparently incorrect view that BSA is "cigar-shaped" at neutral pH.

The results of applying the GA_STRUCT algorithm to the present SANS data at different azoTAB surfactant concentrations, [*S*], and light illumination conditions are shown in Figure 6. At low surfactant concentrations (e.g., 0.55 mM for the trans and 1.60 mM for the cis forms), the heart-shaped structure of BSA is largely unchanged. However, a significant degree of protein unfolding is observed at about 0.80 mM (trans) and 2.21 mM (cis) surfactant concentrations, consistent with the $N \rightarrow F$ transition that was attributed to the triaxial ellipsoid elongation in Table 1, as well as the well-known transition that occurs with decreasing pH (see Figure 1). This increase in the amount of surfactant necessary for the $N \rightarrow F$ transition on going from the trans (more hydrophobic) to the cis (less hydrophobic) forms of azoTAB allows the protein conformation to be controlled with light (see, e.g., $[S] = 1.60$ mM in Figure 6).

The initial unfolding of BSA (throughout the $N \rightarrow F$ transition) apparently involves only the left side (i.e.,

C-terminus part) of the protein, while the right side (N terminus) remains unchanged. This is especially noticeable by observing the bulbous, mushroom-like portion on the upper right of pure BSA, which is still evident even at relatively high surfactant concentrations (2.21 mM for the trans and 7.32 mM for the cis surfactant forms), despite the fact that considerable elongation of the protein has occurred. This is consistent with several experimental studies in the literature that have suggested that the $N \rightarrow F$ transition involves a partial unfolding of the C-terminal (domain III) region, while the N-terminal portion of the protein remains relatively intact (*12*, *26*−*28*).

Continuing increases in the surfactant concentration eventually result in a highly unfolded and elongated protein structure for both the trans ($[S] \geq 2.83$ mM) and cis ($[S] \geq 8.45$ mM) surfactant forms. Again, this is consistent with the $F \rightarrow E$ transition observed with the triaxial fits in Table 1, as well as from the literature with decreases in pH. The analogy between the extent of protein unfolding (i.e., elongation) observed using either model-independent (shape reconstruction) or model-dependent (triaxial ellipsoid) methods also provides for a self-check of the fitting procedures, as well as a high degree of confidence in the results. Further note that, in general, GA_STRUCT predicts an elliptical cross section for BSA, independent of the surfactant concentration, with a thickness (30−50 Å) and width (60−100 Å) more or less consistent with the triaxial ellipsoid fits above. For the unfolded *E* form of BSA, GA_STRUCT gave individual conformations from each of the 10 runs that, despite being similar in the degrees of elongation and unfolding, contained enough variation so as to yield consensus envelopes where much of structure was averaged out. Thus, only the structure for the run best fitting the data is shown in Figure 6 for BSA in the *E* form. To illustrate this effect, the results from two separate runs and the consensus envelope obtained at 5.19 mM azoTAB under visible light are shown in the figure. The detailed evidence of protein unfolding with azoTAB surfactant addition seen in Figure 6, along with the ability to control protein folding reversibly with light illumination, points to the general utility of this SANS analysis technique in protein conformation studies.

In the highly unfolded state, it appears from Figure 6 that the protein is not simply an elongated polymer chain but rather maintains some degree of folding. This is consistent with the observation that even in the most acid-unfolded (*28*) or surfactant-unfolded (*29*) form, BSA still has a significant helical content (∼47%, compared to 65% in the *N* form), primarily because of the 17 disulfide bridges responsible for the 9 loops found in the protein structure. The kinked structures observed in Figure 6 may then be considered consistent with this view of unfolded BSA, representing the helical loops held together by disulfide bonds. Indeed, Takeda et al. have suggested that SDS denaturation does not affect the helices of the six large loops in BSA (*29*). The potential ability to visualize directly the individual subdomains in BSA upon unfolding speaks volumes to the usefulness of SANS in protein-folding studies.

It is important to compare the protein conformations observed in Figure 6 to previous structures deduced from low-angle scattering. There has been some conflicting evidence in the literature, but the most widely held view of

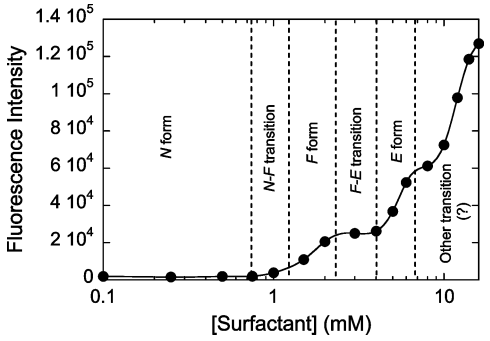

FIGURE 7: Fluorescence intensity of Nile Red in BSA−azoTAB mixtures as a function of the surfactant concentration under visible-light conditions.

the structure of surfactant−protein complexes is the "necklace model" (surfactant micelles arranged along the polypeptide chain) (*2*). Indeed, fractal-like structures consistent with the necklace model have been observed with BSA (*10*, *11*) and lysozyme (*72*) mixed with dodecyl sulfate surfactants. Specifically, for a 1 wt % BSA solution, fractal structures were observed as the surfactant concentration was increased from about 10 to 100 mM (*10*, *11*), significantly higher than the azoTAB concentrations used in the present work. Indeed, it is clear in Figure 4 that the low Q scattering data do not follow a Q^{-d} scaling law that is characteristic of fractal structures with a fractal dimension of d. This is to be expected because comparing the surfactant−protein ratios at 5.19 or 10.34 mM azoTAB (S/P = 34 or 69 mol/mol, respectively) with the aggregation numbers calculated for either free azoTAB micelles ($n = 75$) (*73*), BSA-bound SDS micelles ($n = 29$ or 56) (*4*, *11*), or BSA-bound CTAB micelles ($n \sim 30$) (*74*) at ca. 15 mM surfactant allows for only about one or two micelles per protein, which would clearly not be well-described by a fractal model. It has been suggested that for fractal structures the helical portions of the protein are contained within surfactant micelles [e.g., ref *17* in Ibel et al. (*2*)], consistent with fact that the subdomains of BSA, which are composed of three α helices, contain one face that consists largely of hydrophobic amino acids (*75*). Thus, the kink-like conformations observed in Figure 6 may provide insight into the origin of the fractal structures obtained at higher surfactant concentrations, with the kinks providing seed points onto which micelles grow.

Fluorescence Probes of Surfactant Structure. The possible formation of azoTAB aggregates in the presence of BSA, as well as exposure of the protein hydrophobic domains to the solvent upon unfolding, was probed using the fluorescence dye Nile Red, a hydrophobic probe that exhibits substantial emission increases in response to increasingly hydrophobic microenvironments (*76*, *77*). The increase in fluorescence intensity with the surfactant concentration shown in Figure 7 both corroborates the findings described above and provides additional insight into the way in which the surfactant interacts with the protein. At low surfactant concentrations below about 0.75 mM, the intensity remains low, suggesting that there is little structural rearrangement of the protein and the surfactant does not aggregate on the protein surface. At about 0.75 mM, the fluorescence intensity begins to increase, consistent with a surfactant-induced unfolding of the protein to the *F* form, which causes the hydrophobic domains of the protein to become exposed to

the solvent. Similar increases in Nile Red fluorescence have been observed upon protein unfolding with heat (*78*), surfactant (*79*), or denaturant (*80*). Of particular note is the fact that in mixtures of BSA (0.1 mg/mL) with SDS, Nile Red fluorescence begins to increase beyond surfactant concentrations of 0.70 mM (*79*), similar to the value reported in Figure 7.

Between 0.8 and 2.2 mM azoTAB surfactant concentration, the fluorescence rises rapidly, which can be attributed to solvent exposure of the protein hydrophobic domains that can solubilize Nile Red as the protein unfolds from the *N* to *F* form. At about 2.2 mM, further surfactant addition leads to unfolding of the protein from the *F* to *E* form, consistent with the structures shown in Figure 6 and with the surfactant concentrations responsible for the $N \rightarrow F$ and $F \rightarrow E$ transitions in Table 1. Care must be taken when comparing the SANS results to those in Figure 7. The light scattering and fluorescence measurements were performed at 0.66 mg/mL, because of the need to measure the infinite dilution diffusion coefficient and to maintain a relatively low absorbance, respectively, while the SANS data were for 10 mg/mL to achieve sufficient neutron-scattering count rates. It does appear, however, that the overall surfactant concentration is a key parameter influencing protein unfolding, as judged by the similar trends seen from the three experimental techniques at similar surfactant concentrations. Surfactant binding to proteins generally occurs in two stages: electrostatic binding of the surfactant with oppositely charged amino acids at low surfactant concentrations, followed by cooperative binding because of hydrophobic interactions between the surfactant tails at higher surfactant concentrations. It is the cooperative binding regime, where the number of bound surfactant molecules per protein rapidly increases, which is generally thought to induce protein unfolding (*4*). The surfactant concentration where cooperative binding first begins to occur (termed the critical aggregation concentration in surfactant−polymer systems) is determined primarily by the surfactant hydrophobicity and is largely independent of the polymer concentration (*81*). Thus, it is not surprising that a similar amount of surfactant is required to induce protein unfolding in the three techniques studied, independent of the protein concentration. We estimate that rapid surfactant binding begins to occur beyond the aforementioned seven surfactant molecules bound per protein under visible light determined from preliminary binding isotherms, consistent with the number of high-affinity binding sites on BSA for cationic surfactants (*56*, *57*).

The fluorescence intensity of Nile Red in Figure 7 does not increase substantially again until after 4 mM surfactant has been added to the solution. We attribute this shoulder in the curve between about 2.2 and 4 mM to the adsorption of additional surfactant on the protein, where the surfactant molecules appear to interact independently and associate with the hydrophobic amino acid residues that are now exposed owing to the unfolding of the protein. Above about 4 mM, the protein is fully unfolded to the *E* form and we infer that all exposed hydrophobic groups have been covered by the surfactant; thus, any additional surfactant added to the system leads to the formation of hydrophobic domains on the protein backbone, and the fluorescence intensity increases yet again. It has been noted that it is over this range that the ζ potential becomes increasingly positive, indicating an excess of adsorbed surfactant on the protein. At ~7 mM surfactant, the *E* form becomes saturated with Nile Red and for a brief span of concentrations (7−9 mM) there is no growth in the hydrophobic domains necessary to solubilize more Nile Red. This shoulder in the curve is similar to that observed for the $F \rightarrow E$ transition, and it may indicate the occurrence of further structural changes over this surfactant concentration range, perhaps attributed to some unfolding of one or more of the helical loops or of penetration of these loops by the surfactant. Above 9 mM, however, further increases in surfactant concentration lead to additional solubilization of the dye with consequent large increases in the fluorescence. This is coincident with the peak observed in the SANS spectra at 8 mM surfactant concentration and beyond but cannot be attributed to the formation of micelles either in free solution or on the protein backbone, because the protein-contrasted SANS experiments indicated that such structures do not exist up to at least 20 mM surfactant. Together, these results seem to support that an additional structural change may occur in the BSA−surfactant complex beyond an azoTAB concentration of 8 mM under visible light.

CONCLUSIONS

The ability to control protein folding reversibly with light illumination has been demonstrated through the photoresponsive-surfactant denaturation of BSA. The visible-light (trans) form of the azobenzene surfactant is more hydrophobic than the UV-light (cis) form, and as a consequence, exposing the solutions to visible light results in a greater degree of protein−surfactant interaction and protein elongation, while subsequent exposure to UV light causes the protein to refold. Shape-reconstruction and low-resolution ellipsoidal models used to analyze the SANS data indicate that three discrete forms of the protein are observed depending on the surfactant concentration. Low surfactant concentrations (0−0.55 mM trans and 0−1.60 mM cis) result in a heart-shaped *N* form of BSA in solution, similar to the X-ray crystallographic structure. Intermediate surfactant concentrations (0.80−2.21 mM trans and 2.21−7.32 mM cis) lead to an elongation of BSA to the *F* form, while the $N \rightarrow F$ transition is seen to result primarily from an unfolding of the C-terminus portion of the protein. Finally, at large surfactant concentrations (>2.83 mM trans and >8.45 mM cis), a highly elongated *E* form is evident, although some degree of protein folding remains, consistent with the high helical content of denatured BSA observed in the literature. As a result of these transitions, UV $\leftrightarrow$ visible light illumination can result in reversible $N \leftrightarrow F$ or $F \leftrightarrow E$ protein conformational changes.

ACKNOWLEDGMENT

We thank W. T. Heller for graciously supplying GA_STRUCT, S. R. Kline and B. Hammouda for their help with the SANS data collection and analysis, and S.-H. Chen for helpful insight. We acknowledge the support of the National Institute of Standards and Technology, U.S. Department of Commerce, in providing the neutron research facilities used in this work. This work utilized facilities supported in part by the National Science Foundation under Agreement no. DMR-9986442. We would also like to acknowledge the Cambridge−MIT Institute for support of this research.

REFERENCES

1. Creighton, T. E. (1993) *Proteins: Structure and Molecular Properties*, 2nd ed., W. H. Freeman, New York.
2. Ibel, K., May, R. P., Kirschner, K., Szadkowski, H., Mascher, E., and Lundahl, P. (1990) Protein-decorated micelle structure of sodium-dodecyl-sulfate−protein complexes as determined by neutron scattering, *Eur. J. Biochem. 190*, 311−318.
3. Ananthapadmanabhan, K. P. (1993) in *Interaction of Surfactants with Polymers and Proteins* (Goddard, E. D., and Ananthapadmanabhan, K. P., Eds.) pp 319−365, CRC Press, Boca Raton, FL.
4. Turro, N. J., Lei, X.-G., Ananthapadmanabhan, K. P., and Aronson, M. (1995) Spectroscopic probe analysis of protein−surfactant interactions: The BSA/SDS system, *Langmuir 11*, 2525−2533.
5. Shirahama, K., Tsujii, K., and Takagi, T. (1974) Free-boundary electrophoresis of sodium dodecyl sulfate (SDS)−protein polypeptide complexes with special reference to SDS−polyacrylamide gel electrophoresis, *J. Biochem. 75*, 309−319.
6. Tanford, C. (1980) *The Hydrophobic Effect: Formation of Micelles and Biological Membranes*, 2nd ed., Wiley, New York.
7. Reynolds, J. A., and Tanford, C. (1970) Gross conformation of protein−sodium dodecyl sulfate complexes, *J. Biol. Chem. 245*, 5161−5165.
8. Lundahl, P., Greijer, E., Sandberg, M., Cardell, S., and Eriksson, K. O. (1986) A model for ionic and hydrophobic interactions and hydrogen-bonding in sodium dodecyl sulfate−protein complexes, *Biochim. Biophys. Acta 873*, 20−26.
9. Tanner, R. E., Herpigny, B., Chen, S. H., and Rha, C. K. (1982) Conformational change of protein sodium dodecyl sulfate complexes in solution: A study of dynamic light scattering, *J. Chem. Phys. 76*, 3866−3872.
10. Chen, S. H., and Teixeira, J. (1986) Structure and fractal dimension of protein−detergent complexes, *Phys. Rev. Lett. 57*, 2583−2586.
11. Santos, S. F., Zanette, D., Fischer, H., and Itri, R. (2003) A systematic study of bovine serum albumin (BSA) and sodium dodecyl sulfate (SDS) interactions by surface tension and small-angle X-ray scattering, *J. Colloid Interface Sci. 262*, 400−408.
12. Carter, D. C., and Ho, J. X. (1994) Structure of serum albumin, *Adv. Protein Chem. 45*, 153−203.
13. Peters, T., Jr. (1985) Serum albumin, *Adv. Protein Chem. 37*, 161−245.
14. Brown, J. R. (1977) in *Albumin Structure, Function, and Uses* (Rosenoer, V. M., Oratz, M., and Rothschild, M. A., Eds.) pp 27−51, Pergamon, Oxford, U.K.
15. Peters, T. J. (1996) *All about Albumin*, Academic Press, San Diego.
16. Oncley, J. L., Scatchard, G., and Brown, A. (1947) Physicochemical characteristics of certain of the proteins of normal human plasma, *J. Phys. Colloid Chem. 51*, 184−198.
17. Tanford, C., and Buzzell, J. G. (1956) The viscosity of aqueous solutions of bovine serum albumin between pH 4.3 and 10.5, *J. Phys. Chem. 60*, 225−231.
18. Champagne, M. (1957) The structure of serum albumin in dilute solution. I. Serum albumin at the isoionic point, *J. Chim. Phys. 54*, 378−392.
19. Squire, P. G., Moser, P., and O'Konski, C. T. (1968) Hydrodynamic properties of bovine serum albumin monomer and dimer, *Biochemistry 7*, 4261−4272.
20. Wright, A. K., Thompson, M. R., and Miller, R. L. (1975) A study of protein−sodium dodecyl sulfate complexes by transient electric birefringence, *Biochemistry 14*, 3224−3228.
21. Luzzati, V., Witz, J., and Nicolaieff, A. (1961) The structure of bovine serum albumin in solution at pH 5.3 and 3.6; study by absolute scattering of X-rays, *J. Mol. Biol. 3*, 379−392.
22. Bloomfield, V. (1966) The structure of bovine serum albumin at low pH, *Biochemistry (Moscow) 5*, 684−689.
23. Feng, L., Hu, C. Z., and Andrade, J. D. (1988) Scanning tunneling microscopic images of adsorbed serum albumin on highly oriented pyrolytic graphite, *J. Colloid Interface Sci. 126*, 650−653.
24. Ferrer, M. L., Duchowicz, R., Carrasco, B., Garcia de la Torre, J., and Acuna, A. U. (2001) The conformation of serum albumin in solution: A combined phosphorescence depolarization-hydrodynamic modeling study, *Biophys. J. 80*, 2422−2430.
25. He, X. M., and Carter, D. C. (1992) Atomic structure and chemistry of human serum albumin, *Nature 358*, 209−215.
26. Jones, M. N., Skinner, H. A., and Tipping, E. (1975) The interaction between bovine serum albumin and surfactants, *Biochem. J. 147*, 229−234.
27. Geisow, M. J., and Beaven, G. H. (1977) Physical and binding properties of large fragments of human serum albumin, *Biochem. J. 163*, 477−484.
28. Khan, M. Y. (1986) Direct evidence for the involvement of domain III in the N−F transition of bovine serum albumin, *Biochem. J. 236*, 307−310.
29. Takeda, K., Moriyama, Y., and Hachiya, K. (2002) in *Encyclopedia of Surface and Colloid Science* (Hubbard, A. T., and Somasundaran, P., Eds.) pp 2558−2574, Marcel Dekker, New York.
30. Hayashita, T., Kurosawas, T., Miyata, T., Tanaka, K., and Igawa, M. (1994) Effect of structural variation within cationic azo-surfactant upon photoresponsive function in aqueous solution, *Colloid Polym. Sci. 272*, 1611−1619.
31. Shin, J. Y., and Abbott, N. L. (1999) Using light to control dynamic surface tensions of aqueous solutions of water soluble surfactants, *Langmuir 15*, 4404−4410.
32. Eastoe, J., Dominguez, M. S., Wyatt, P., Beeby, A., and Heenan, R. K. (2002) Properties of a stilbene-containing gemini photosurfactant: Light-triggered changes in surface tension and aggregation, *Langmuir 18*, 7837−7844.
33. Eastoe, J., Sanchez-Dominguez, M., Cumber, H., Burnett, G., Wyatt, P., and Heenan, R. K. (2003) Photoresponsive microemulsions, *Langmuir 19*, 6579−6581.
34. Shang, T., Smith, K. A., and Hatton, T. A. (2003) Photoresponsive surfactants exhibiting unusually large, reversible surface tension changes under varying illumination conditions, *Langmuir 19*, 10764−10773.
35. Lee, C. T., Smith, K. A., and Hatton, T. A. (2004) Photoreversible viscosity changes and gelation in mixtures of hydrophobically-modified polyelectrolytes and photosensitive surfactants, *Macromolecules 37*, 5397−5405.
36. Glinka, C. J., Barker, J. G., Hammouda, B., Krueger, S., Moyer, J. J., and Orts, W. J. (1998) The 30 m small-angle neutron scattering instruments at the National Institute of Standards and Technology, *J. Appl. Crystallogr. 31*, 430−445.
37. Svergun, D. I. (1992) Determination of the regularization parameter in indirect-transform methods using perceptual criteria, *J. Appl. Crystallogr. 25*, 495−503.
38. Bendedouch, D., and Chen, S. H. (1983) Structure and interparticle interactions of bovine serum albumin in solution studied by small-angle neutron scattering, *J. Phys. Chem. 87*, 1473−1477.
39. Mittelbach, P., and Porod, G. (1962) Small-angle X-ray scattering of dilute colloids. VII. Distribution functions of triaxial ellipsoids, *Acta Phys. Austriaca 15*, 122−147.
40. Feigin, L. A., and Svergun, D. I. (1987) *Structure Analysis by Small-Angle X-ray and Neutron Scattering*, Plenum Press, New York.
41. Bergstrom, M., and Skov Pedersen, J. (1999) Structure of pure SDS and DTAB micelles in brine determined by small-angle neutron scattering (SANS), *Phys. Chem. Chem. Phys. 1*, 4437−4446.
42. Hayter, J. B., and Penfold, J. (1981) An analytic structure factor for macroion solutions, *Mol. Phys. 42*, 109−118.
43. Hansen, J. P., and Hayter, J. B. (1982) A rescaled MSA structure factor for dilute charged colloidal dispersions, *Mol. Phys. 46*, 651−656.
44. Sharma, R. V., and Sharma, K. C. (1977) The structure factor and the transport properties of dense fluids having molecules with square well potential, a possible generalization, *Physica A 89*, 213−218.
45. Tardieu, A., Le Verge, A., Malfois, M., Bonnete, F., Finet, S., Ries-Kautt, M., and Belloni, L. (1999) Proteins in solution: From X-ray scattering intensities to interaction potentials, *J. Cryst. Growth 196*, 193−203.
46. Heller, W. T., Krueger, J. K., and Trewhella, J. (2003) Further insights into calmodulin-myosin light chain kinase interaction from solution scattering and shape restoration, *Biochemistry 42*, 10579−10588.
47. Oh, Y. S., and Johnson, C. S., Jr. (1981) The wave vector dependence of diffusion coefficients in photon correlation spectroscopy of protein solutions, *J. Chem. Phys. 74*, 2717−2720.
48. Gaigalas, A. K., Hubbard, J. B., McCurley, M., and Woo, S. (1992) Diffusion of bovine serum albumin in aqueous solutions, *J. Phys. Chem. 96*, 2355−2359.
49. Takeda, K., Sasaoka, H., Sasa, K., Hirai, H., Hachiya, K., and Moriyama, Y. (1992) Size and mobility of sodium dodecyl sulfate−bovine serum albumin complex as studied by dynamic light scattering and electrophoretic light scattering, *J. Colloid Interface Sci. 154*, 385−392.

50. Chen, A., Wu, D., and Johnson, C. S., Jr. (1995) Determination of the binding isotherm and size of the bovine serum albumin−sodium dodecyl sulfate complex by diffusion-ordered 2D NMR, *J. Phys. Chem. 99*, 828−834.
51. Meechai, N., Jamieson, A. M., and Blackwell, J. (1999) Translational diffusion coefficients of bovine serum albumin in aqueous solution at high ionic strength, *J. Colloid Interface Sci. 218*, 167−175.
52. Valstar, A., Almgren, M., Brown, W., and Vasilescu, M. (2000) The interaction of bovine serum albumin with surfactants studied by light scattering, *Langmuir 16*, 922−927.
53. Kirkwood, J. G. (1954) The general theory of irreversible processes in solutions of macromolecules, *J. Polym. Sci. 12*, 1−14.
54. Bloomfield, V. A., Dalton, W. O., and van Holde, K. E. (1967) Frictional coefficients of multisubunit structures. I. Theory, *Biopolymers 5*, 135−148.
55. Slayter, E. M. (1965) An electron microscope study of the conformational change in bovine serum albumin at low pH, *J. Mol. Biol. 14*, 443−452.
56. Nozaki, Y., Reynolds, J. A., and Tanford, C. (1974) Interaction of a cationic detergent with bovine serum albumin and other proteins, *J. Biol. Chem. 249*, 4452−4459.
57. Kaneshina, S., Tanaka, M., Kondo, T., Mizuno, T., and Aoki, K. (1973) Interaction of bovine serum albumin with detergent cations, *Bull. Chem. Soc. Jpn. 46*, 2735−2738.
58. Glatter, O. (1977) A new method for the evaluation of small-angle scattering data, *J. Appl. Crystallogr. 10*, 415−421.
59. Svergun, D. I., Petoukhov, M. V., and Koch, M. H. J. (2001) Determination of domain structure of proteins from X-ray solution scattering, *Biophys. J. 80*, 2946−2953.
60. Sjoeberg, B., and Mortensen, K. (1997) Structure and thermodynamics of nonideal solutions of colloidal particles: Investigation of salt-free solutions of human serum albumin by using small-angle neutron scattering and Monte Carlo simulation, *Biophys. Chem. 65*, 75−83.
61. Kiselev, M. A., Gryzunov Iu, A., Dobretsov, G. E., and Komarova, M. N. (2001) Size of a human serum albumin molecule in solution, *Biofizika 46*, 423−427.
62. Velev, O. D., Kaler, E. W., and Lenhoff, A. M. (1998) Protein interactions in solution characterized by light and neutron scattering: Comparison of lysozyme and chymotrypsinogen, *Biophys. J. 75*, 2682−2697.
63. Ninio, J., Luzzati, V., and Yaniv, M. (1972) Comparative small-angle X-ray scattering studies on unacylated, acylated, and crosslinked *Escherichia coli* transfer RNAIVa1, *J. Mol. Biol. 71*, 217−229.
64. Timchenko, A. A., Ptitsyn, O. B., Dolgikh, D. A., and Fedorov, B. A. (1978) The structure of ribonuclease in solution does not differ from its crystalline structure, *FEBS Lett. 88*, 105−108.
65. Fedorov, B. A., and Denesyuk, A. I. (1978) Large-angle X-ray diffuse scattering, a new method for investigating changes in the conformation of globular proteins in solutions, *J. Appl. Crystallogr. 11*, 473−477.
66. Pavlov, M. Y., Sinev, M. A., Timchenko, A. A., and Ptitsyn, O. B. (1986) A study of apo- and holo-forms of horse liver alcohol dehydrogenase in solution by diffuse X-ray scattering, *Biopolymers 25*, 1385−1397.
67. Heidorn, D. B., and Trewhella, J. (1988) Comparison of the crystal and solution structures of calmodulin and troponin C, *Biochemistry 27*, 909−915.
68. Durchschlag, H., and Zipper, P. (1996) Comparative determination of structural parameters and conformational changes of proteins by small-angle scattering, crystallography, and hydrodynamic analysis, *J. Mol. Struct. 383*, 223−229.
69. Tanford, C. (1950) Preparation and properties of serum and plasma proteins. XXIII. Hydrogen-ion equilibria in native and modified human serum albumins, *J. Am. Chem. Soc. 72*, 441−451.
70. Hunter, M. J. (1966) A method for the determination of protein partial specific volumes, *J. Phys. Chem. 70*, 3285−3292.
71. Kuntz, I. D., Jr., and Kauzmann, W. (1974) Hydration of proteins and polypeptides, *Adv. Protein Chem. 28*, 239−345.
72. Stenstam, A., Montalvo, G., Grillo, I., and Gradzielski, M. (2003) Small angle neutron scattering study of lysozyme−sodium dodecyl sulfate aggregates, *J. Phys. Chem. B 107*, 12331−12338.
73. Lee, C. T., Smith, K. A., and Hatton, T. A. (2004) Small-angle neutron scattering (SANS) studies of photosensitive surfactant-polyelectrolyte gels, in progress.
74. Vasilescu, M., Angelescu, D., Almgren, M., and Valstar, A. (1999) Interactions of globular proteins with surfactants studied with fluorescence probe methods, *Langmuir 15*, 2635−2643.
75. Brown, J. R., and Scockley, P. (1982) in *Lipid−Protein Interactions* (Jost, P. C., and Griffith, O. H., Eds.) pp 25−68, Wiley, New York.
76. Sarkar, N., Das, K., Nath, D. N., and Bhattacharyya, K. (1994) Twisted charge-transfer processes of Nile Red in homogeneous solutions and in faujasite zeolite, *Langmuir 10*, 326−329.
77. Dutta, A. K., Kamada, K., and Ohta, K. (1996) Spectroscopic studies of Nile Red in organic solvents and polymers, *J. Photochem. Photobiol., A 93*, 57−64.
78. Sackett, D. L., and Wolff, J. (1987) Nile red as a polarity-sensitive fluorescent probe of hydrophobic protein surfaces, *Anal. Biochem. 167*, 228−234.
79. Daban, J. R., Samso, M., and Bartolome, S. (1991) Use of Nile Red as a fluorescent probe for the study of the hydrophobic properties of protein−sodium dodecyl sulfate complexes in solution, *Anal. Biochem. 199*, 162−168.
80. Santra, M. K., Banerjee, A., Krishnakumar, S. S., Rahaman, O., and Panda, D. (2004) Multiple-probe analysis of folding and unfolding pathways of human serum albumin. Evidence for a framework mechanism of folding, *Eur. J. Biochem. 271*, 1789−1797.
81. Jönsson, B., Lindman, B., Holmberg, K., and Kronberg, B. (1998) in *Surfactants and Polymers in Aqueous Solutions*, pp 219−245, Wiley, New York.

BI048556C